Organic Electronics 10 (2009) 1636–1640

Contents lists available at ScienceDirect

Organic Electronics

journal homepage: www.elsevier.com/locate/orgel

Letter

Using metal/organic junction engineering to prepare an efficient organic base-modulation triode and its inverter

Shiau-Shin Cheng [a], Jia-Hao Chen [a], Guan-Yuan Chen [a], Dhananjay Kekuda [b], Meng-Chyi Wu [a], Chih-Wei Chu [b,c,*]

[a] Department of Electrical Engineering, National Tsing-Hua University, Hsinchu 30013, Taiwan
[b] Research Center for Applied Sciences, Academia Sinica, Taipei 11529, Taiwan
[c] Department of Photonics, National Chiao-Tung University, Hsinchu 30010, Taiwan

ARTICLE INFO

Article history:
Received 22 June 2009
Received in revised form 27 August 2009
Accepted 28 August 2009
Available online 3 September 2009

PACS:
72.80.Le
84.37.+q
73.61.Ph
06.60.Jn

Keywords:
Vertical-type
Junction
Transition metal oxide
Inverter

ABSTRACT

In this study, we investigated the influence of a buffer layer of molybdic oxide (MoO_3) at the metal/organic junction on the behavior of organic base-modulation triodes. The performance of devices featuring MoO_3/Al as the emitter electrode was enhanced relative to that of corresponding devices with Au and Ag, presumably because of the reduced in the contact barrier and the prevention of metal diffusion into the organic layer. The device exhibited an output current of −16.1 μA at V_B = −5 V and a current ON/OFF ratio of 10^3. Using this architecture, we constructed resistance–load inverters that exhibited a calculated gain of 6.

1. Introduction

The low cost and mechanical flexibility of organic thin-film transistors (OTFTs) have attracted much scientific and industrial interest for their use in the development of "plastic" electronics, such as flat-panel display drivers, radio-frequency identification tags, and sensors [1–5]. Although many research groups have synthesized a diverse range of organic semiconductors for use in planar-type OTFTs, these devices still require high driving voltages and exhibit slow operation speeds because of low mobilities. Several approaches have been developed to overcome these issues, including the use of high-*k* dielectrics [6,7] and reducing the channel length of the devices [8,9]. The preparation of high-*k* dielectric thin-films requires high-temperature processing; the resulting rough surfaces of the organic semiconductors usually exhibit decreased crystallinity and increased leakage currents. The disadvantage of reducing the channel length is that the contact resistance of the semiconductor/metal interface limits the performance of the device. An alternative approach toward lowering the driving voltage and increasing the speed of devices, while using existing organic semiconductors as channel materials, is to fabricate vertical-type transistors in which the channel length can controlled precisely down to the nano-scale [10–18].

* Corresponding author. Address: Research Center for Applied Sciences, Academia Sinica, Taipei 11529, Taiwan. Tel.: +886 2 27898000x70; fax: +886 2 27826680.
E-mail address: gchu@gate.sinica.edu.tw (C.-W. Chu).

1566-1199/$ - see front matter © 2009 Elsevier B.V. All rights reserved.
doi:10.1016/j.orgel.2009.08.023

The junction between the electrode and the organic semiconductor has a significant influence on the performance of an organic device [19]. A buffer layer is usually sandwiched at the metal–organic semiconductor interface to improve the charge-injection capability and overall device performance [20–22]. Although the output current in vertical-type transistors is dramatically enhanced when a thin buffer layer of LiF is incorporated between the emitter electrode and the organic emitter [13,23], the OFF current usually remains high – sometimes even higher than that of the device lacking a LiF layer. This behavior might be attributable to the diffusion of metal into the active layer or unfavorable chemical reactions between the organic layer and the metal electrode when operating the devices under high electric fields. Moreover, because the leakage current of a vertical transistor depends mainly on its film thickness, the presence of a thin LiF layer cannot help to reduce the leakage current. Hence, the choice of the buffer layer is a crucial factor toward improving the overall device performance.

Employing the diverse electronic properties of transition metal oxides could provide a unique opportunity to lower the energy barrier between metal and organic for the charge-injection. When a metal oxide film is sandwiched between the metal and organic semiconductor, the fundamental principle governing charge-injection at the junction is controlled by the doping concentration of the film. Therefore, a thicker film can be incorporated to prevent the diffusion of metal into the active layer and unfavorable chemical reactions between the active layer and metal electrode, while maintaining the charge-injection capability. In this Letter, we describe how the performance of organic base-modulation triodes (OBMTs) is improved after inserting a metal oxide film between the emitter electrode and the organic emitter. The OBMTs featuring molybdic oxide (MoO_3)/Al bilayer emitter electrodes exhibited increased output current; as a result, the current ON/OFF ratio reached as high as 10^3, thereby allowing inverters to be prepared exhibiting higher gains.

2. Experimental

The structure of the OBMTs is revealed in the inset to Fig. 1. Prior to deposition, the glass substrates were cleaned using detergent, acetone, and isopropyl alcohol and then treated in a UV–ozone cleaner for 15 min. A 30-nm-thick Au layer was deposited on the glass substrate to serve as a collector electrode. A 50-nm-thick layer of copper phthalocyanine (CuPc, Luminescence Technology) was thermal deposited on the Au layer to smoother the surface morphology and then a 270-nm-thick layer of pentacene (ca. 98% purity, Luminescence Technology), which served as the collector of the p-channel triode, was thermal evaporated. A 30-nm-thick Al strip was thermally evaporated onto the pentacene layer to function as the base electrode. A thin Al film (10 nm) was then deposited and a lithium fluoride (LiF) layer of 0.4 nm was thermally evaporated to function as a hole injection enhancement layer. A 20-nm-thick layer of *N*,*N*′-bis(naphthalen-1-yl)-*N*,*N*′-bisphenylbenzidine (NPB) was thermally evaporated to enhance the carrier energy. Pentacene was then thermally evaporated to form the 100-nm-thick emitter layer. Finally, for comparison, three types of emitter electrodes were used: 30-nm-thick Au, 30-nm-thick Ag, and 50-nm-thick MoO_3/30-nm-thick Al. The patterns of each layer were defined using different metallic shadow masks. The active area of the device, defined by the crossover between the emitter and collector electrodes, was 0.0042 cm^2. The work functions of Al, Au, and Ag and the energy level of MoO_3 are presented schematically in Fig. 2a [20]. All organic materials were used without further purification and were deposited through thermal evaporation at a base pressure of ca. 2×10^{-6} torr. The current–voltage (I–V) characteristics of the devices in a glove-box ambient (H_2O and O_2 contents: <1 ppm) were measured using a Keithley 4200 semiconductor parameter analyzer. X-ray photoelectron spectroscopy (XPS) was performed using a PHI 5000 VersaProbe system (ULVAC-PHI Chigasaki, Japan) and a microfocused (100 μm, 25 W) Al X-ray beam with a photoelectron take-off angle of 45°.

3. Results and discussion

Fig. 1a displays the collector-to-emitter current (I_{CE}) versus the collector-to-emitter voltage (V_{CE}) characteristics of the OBMT employing MoO_3/Al as the emitter electrode, with base–emitter voltages (V_{BE}) ranging from 0 to −5 V at a step of 0.5 V. The value of I_{CE} reached up to −16.1 μA when V_{CE} and V_{BE} were both −5 V. The current ON/OFF ratio, defined as I_{CE} (V_{BE} = −5 V)/I_{CE} (V_{BE} = 0 V) at V_{CE} = −5 V, was ca. 3.08×10^3. For comparison, we also tested Au and Ag as emitter electrodes. We found that the emitter electrode of the emitter–base (EB) diode had a significant influence on the electronic properties of the OBMTs. Table 1 summarizes the device parameters of the OBMTs employing Au, Ag, and MoO_3/Al as emitter electrodes. The device featuring MoO_3/Al as the emitter electrode had the highest ON current, while maintaining an OFF current similar to those of the other systems. Although a small energy barrier exits between Au and pentacene, metals deposited onto the pentacene surface penetrate the surface, thereby doping the upper layer of pentacene to form a metallic overlayer. Due to charge transfer across the metal/organic semiconductor interface, redistribution of electron cloud, and interfacial chemical reaction, an interface dipole forms immediately, increasing the barrier height between the metal and pentacene [24,25]. The modified MoO_3 layer interface provided protection against metal diffusion into the organic layer and unfavorable chemical reactions between the organic and metal electrodes; it decreased the intensity of the interface dipole and enhanced the degree of charge-injection. Besides, we also observed the output current of the device was modulated by the base current. Fig. 1b and c displays the I_{CE} versus V_{CE} under common-base mode and common-emitter mode. As the following two equations [16]:

$$\alpha = \frac{I_{CE} - I_{CE}(I_E = 0A)}{I_E} \quad (1)$$

$$\beta = \frac{I_{CE} - I_{CE}(I_B = 0A)}{I_B} \quad (2)$$

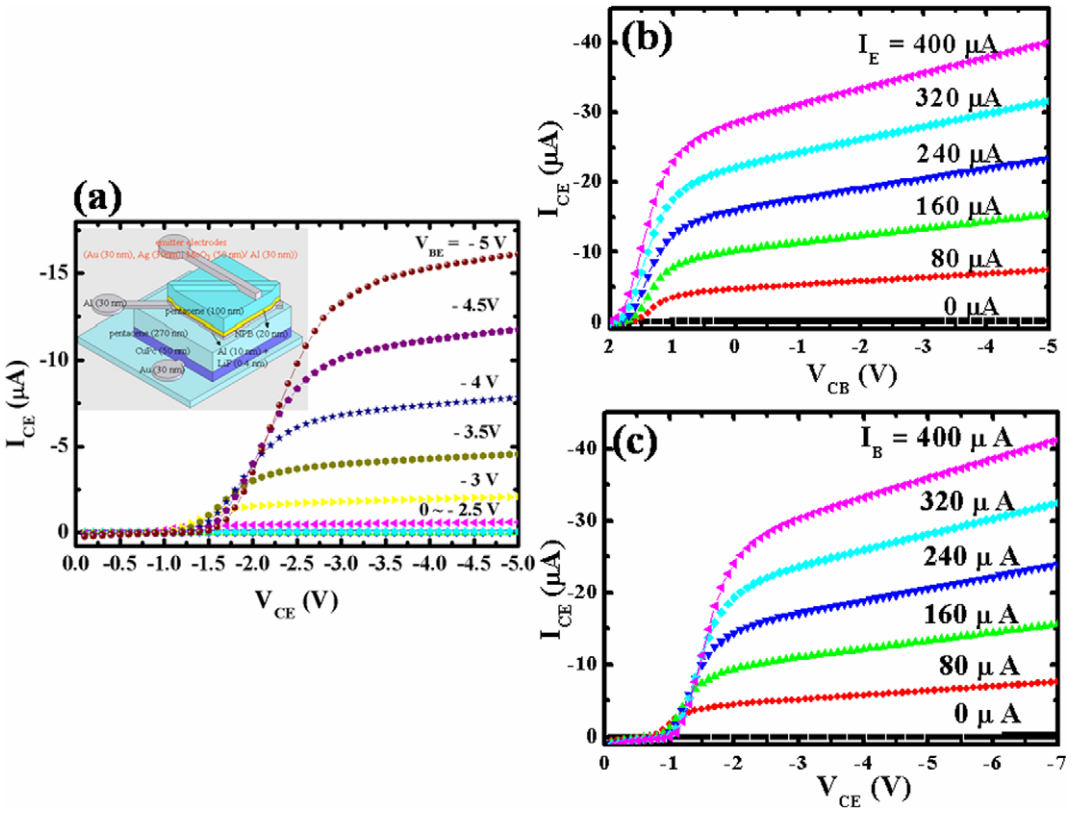

Fig. 1. (a) Collector-to-emitter current (I_{CE}) plotted as a function of the collector-to-emitter voltage (V_{CE}) for base voltages ranging from 0 to −5 V at a step of −0.5 V. (b) I_{CE} as a function of V_{CE} for emitter current ranging from 0 to 400 μA under the common-base mode. (c) I_{CE} as a function of V_{CE} for base current ranging from 0 to 400 μA under the common-emitter mode. Inset: schematic representation of the device structure with emitter electrode MoO_3/Al.

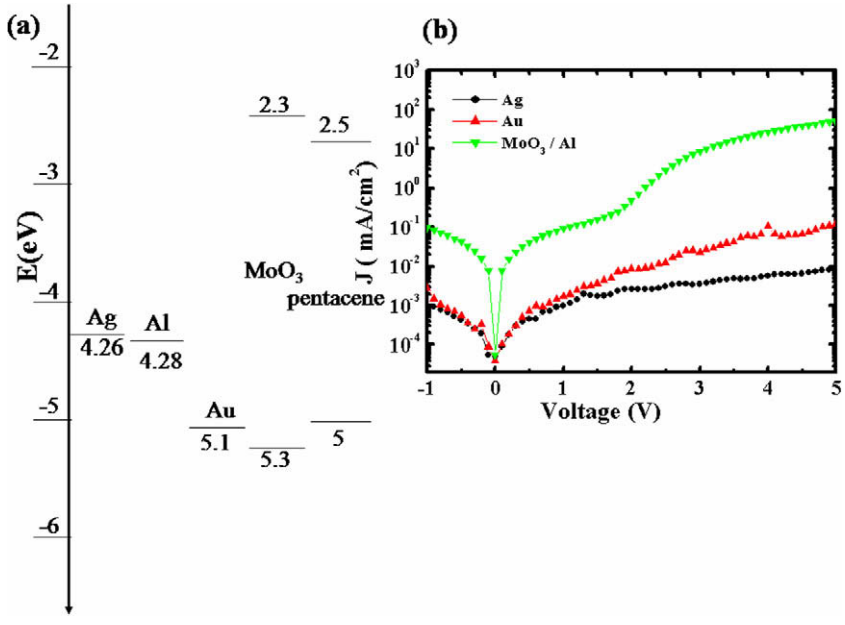

Fig. 2. (a) Current density (J) versus voltage (V) characteristics of EB diodes featuring Au, Ag, and MoO_3/Al as emitter electrodes. (b) Energy level diagrams of the organic materials and the metals.

The I_E and I_B are the input emitter current and the base current under common-base and common-emitter mode, respectively. Under Eqs. (1) and (2), the transport factor (α) of 0.1 and current gain (β) of 0.1 were measured. To determine the reason why the barrier between the electrode and organic layer influenced the performance of

Table 1
Device performance of OBMTs featuring Au, Ag, and MoO_3/Al as emitter electrodes; V_{CE} and V_B were both −5 V.

Emitter electrode	Output current (A)	OFF current (A)	Current ON/OFF ratio
Au	3.51×10^{-6}	4.42×10^{-9}	7.94×10^{2}
Ag	1.29×10^{-8}	5.43×10^{-9}	2.37
MoO_3/Al	1.61×10^{-5}	5.23×10^{-9}	3.08×10^{3}

the OBMTs, we measured the current density (J) versus voltage (V) characteristics of EB diodes featuring Au, Ag, and MoO_3/Al as emitter electrodes. Fig. 2b reveals that the EB diode incorporating the MoO_3 layer provided improved hole injection and an obvious turn-on effect at ca. 1.4 V in Fig. 1 when V_{BE} was −5 V. For the same CB diode structure, the output current of the OBMT is determined by the currents of the forward-bias EB diode and the reverse-bias CB diode [18]. Therefore, the output current of the OBMTs was enhanced when using MoO_3/Al as the emitter electrode.

Because we deposited the MoO_3 layer through thermal evaporation, inevitably it decomposed into various Mo species. We recorded XPS spectra to identify the chemical species present in the "MoO_3" layer (Fig. 3). In Fig. 3b, we observe two measured binding energies (228.5 and 231.5 eV), suggesting that the layer included two or more Mo species. Contamination from the boat introduced into the film during thermal evaporation resulted in the shifting of the two peaks [26] from their expected values for MoO_3 and MoO_2 [27]. The intensities of the signals for MoO_2 and MoO_3 were similar, suggesting that MoO_2 was heavily doped into the MoO_3 film. Therefore, the MoO_3 film behaved as a degenerate semiconductor, to align the work function of the metal and the Fermi-level of the MoO_3 layer, with the depletion region at the MoO_3–Al interface being so narrow that the carriers had a high probability of tunneling through the barrier when a suitable bias voltage was applied to the EB diode. To further demonstrate this phenomenon, we fabricated emitter electrodes featuring different thicknesses of the MoO_3 interfacial layer; Fig. 4 presents the J–V characteristics of the resulting EB

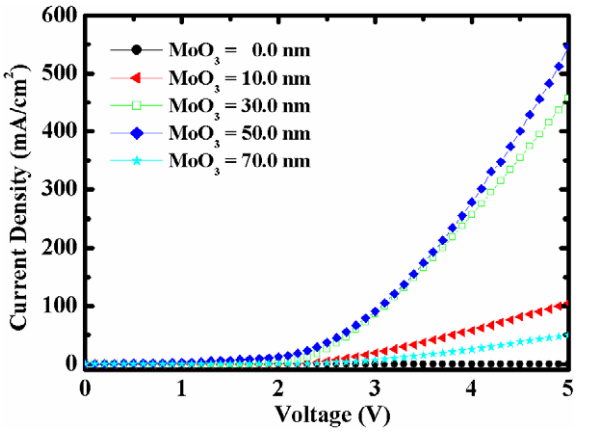

Fig. 4. Current density (J) versus voltage (V) characteristics of EB diodes having the structure Al (30 nm)/thin Al (10 nm)/LiF (0.4 nm)/NPB (20 nm)/pentacene (100 nm)/MoO_3 (0–70 nm)/Al (30 nm).

diodes. The devices employing MoO_3/Al bilayers had larger current densities than that featuring the bare Al layer; the maximum value occurred at a MoO_3 thickness of 50 nm. Because a thicker MoO_3 interfacial layer would result in a longer carrier transport pathway, the probability of carrier capture would increase rapidly and the number of carriers received by the electrode would decrease. Therefore, OBMTs employing a suitable MoO_3 thickness would provide superior hole–injection contact and enhance the output current of the EB diode.

One of the advantages of the OBMTs requiring voltage driving is that they can be used to construct organic inverters. Fig. 5a and b displays the measured transfer characteristics of organic inverters composed of the OBMT connected with various resistances and corresponding gains, respectively. The resistance ranged from 2 to 10 MΩ at a step of 2 MΩ; a supply voltage of −5 V was applied. The inset displays the structure of a vertical OBMT with a load resistor. The corresponding gain of the inverter changed with respect to the resistance, with a maximum calculated gain of 6 arising when the OBMT was connected with a resistance of 10 MΩ. This resistor is, however, not an ideal switch; it resulted in the value of V_{out} of the inver-

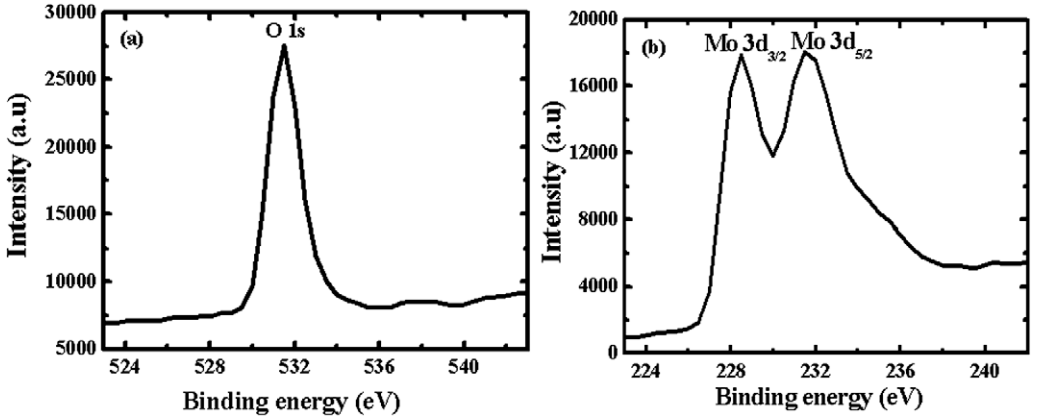

Fig. 3. XPS spectra of the (a) O 1s and (b) Mo 3d energy levels.

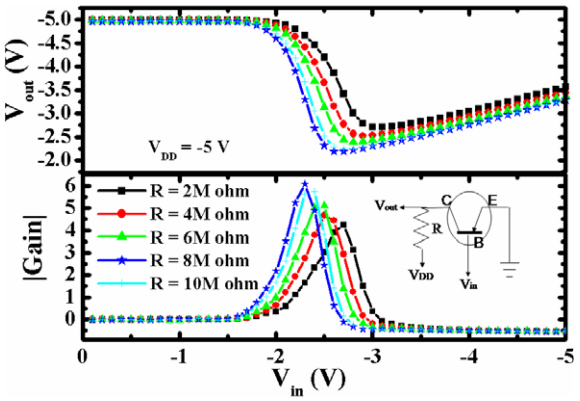

Fig. 5. Measured transfer characteristics and corresponding gain of inverters measured at a value of V_{DD} of −5 V with resistances ranging from 2 to 10 MΩ at a step of 2 MΩ. Inset: sketch of the inverter structure and OBMT employing MoO_3/Al as emitter electrode.

ter varying upon increasing $|V_{in}|$. To overcome this drawback, the n-type OBMT should replace the resistor to form a complementary inverter; such a study is currently under investigation.

4. Conclusion

In conclusion, we have fabricated OBMTs featuring three types of emitter electrodes (Au, Ag, and MoO_3/Al). The output currents of these OBMTs were strongly related to the nature of the interface between the emitter electrode and the organic semiconductor layer. XPS analysis revealed that the MoO_3 films formed through thermal evaporation had degenerate semiconductor characteristics, resulting in a tunnel current component at the EB diode. Therefore, the devices featuring MoO_3/Al as the emitter electrode exhibited a current ON/OFF ratio of 10^3. Connecting different resistances to the OBMT allowed us to prepare inverters.

Acknowledgment

This study was supported in part by the National Science Council, Taiwan, under grants NSC 97-2628-E-007-026-MY2 and NSC 98-2221-E-001-002.

References

[1] M.G. Kane, J. Campi, M.S. Hammond, F.P. Cuomo, B. Greening, C.D. Sheraw, J.A. Nichols, D.J. Gundlach, J.R. Huang, C.C. Kuo, L. Jia, H. Klauk, T.N. Jackson, IEEE Electron Device Lett. 21 (2000) 34.
[2] C.J. Drury, C.M.J. Mutsaers, C.M. Hart, M. Matters, D.M. deLeeuw, Appl. Phys. Lett. 73 (1998) 108.
[3] C.D. Dimitrakopoulos, P.R.L. Malenfant, Adv. Mater. 14 (2002) 99.
[4] D.J. Monsma, J.C. Lodder, T.J.A. Popma, B. Dieny, Phys. Rev. Lett. 74 (1995) 5260.
[5] P.F. Baude, D.A. Ender, M.A. Haase, T.W. Kelley, D.V. Muyres, S.D. Theiss, Appl. Phys. Lett. 82 (2003) 3964.
[6] C.D. Dimitrakopoulos, S. Purushothaman, J. Kymissis, A. Callegari, J.M. Shaw, Science 283 (1999) 822.
[7] F.C. Chen, C.S. Chuang, Y.S. Lin, L.J. Kung, T.H. Chen, H.P. Shieh, Org. Electron. 7 (2006) 435.
[8] Y.Y. Noh, N. Zhao, M. Caironi, H. Sirringhaus, Nat. Nanotechnol. 2 (2007) 784.
[9] M.D. Austin, S.Y. Chou, Appl. Phys. Lett. 81 (2002) 4431.
[10] K. Kudo, M. Iizuka, S. Kuniyoshi, K. Tanaka, Thin Solid Films 393 (2001) 362.
[11] Y. Yang, A.J. Heeger, Nature 372 (1994) 344.
[12] M.S. Meruvia, I.A. Hummelgen, M.L. Sartorelli, A.A. Pasa, W. Schwarzacher, Appl. Phys. Lett. 84 (2004) 3978.
[13] K. Nakayama, S. Fujimoto, M. Yokoyama, Appl. Phys. Lett. 88 (2006) 153512.
[14] S.H. Li, Z. Xu, L.P. Ma, Y. Yang, Appl. Phys. Lett. 91 (2007) 083507.
[15] Y.C. Chao, M.H. Xie, M.Z. Dai, H.F. Meng, S.F. Horng, C.S. Hsu, Appl. Phys. Lett. 92 (2008) 093310.
[16] C.Y. Yang, T.M. Ou, S.S. Cheng, M.C. Wu, S.Y. Lin, I.M. Chan, Y.J. Chan, Appl. Phys. Lett. 89 (2006) 183511.
[17] S.S. Cheng, C.Y. Yang, Y.C. Chuang, C.W. Ou, M.C. Wu, S.Y. Lin, Y.J. Chan, Appl. Phys. Lett. 90 (2007) 153509.
[18] S.S. Cheng, Y.C. Chuang, D. Kekuda, C.W. Ou, M.C. Wu, C.W. Chu, Adv. Mater. 21 (2009) 1860.
[19] H. Ishii, K. Sugiyama, E. Ito, K. Seki, Adv. Mater. 8 (1999) 11.
[20] C.W. Chu, S.H. Li, C.W. Chen, V. Shrotriya, Y. Yang, Appl. Phys. Lett. 87 (2005) 193508.
[21] L.S. Hung, C.W. Tang, M.G. Mason, Appl. Phys. Lett. 70 (1997) 152.
[22] G.L. Frey, K.J. Reynolds, R.H. Friend, Adv. Mater. 14 (2002) 265.
[23] L.S. Roman, W. Mammo, L.A.A. Pettersson, M.R. Andersson, O. Inganäs, Adv. Funct. Mater. 10 (1998) 774.
[24] N.J. Watkins, L. Yan, Y.L. Gao, Appl. Phys. Lett. 80 (2002) 4384.
[25] H. Ishii, K. Sugiyama, E. Ito, Kazuhiko Seki, Adv. Mater. 11 (1999) 605.
[26] G.D. Giuseppe, J.R. Selman, J. Electronanal. Chem. 559 (2003) 31.
[27] J.F. Moulder, W.F. Stickle, P.E. Sobol, K.D. Bomben, J. Chastin, in: Handbook of X-ray Photoelectron Spectroscopy, Perkin–Elmer Corporation, Physical Electronics Division, Minnesota, 1992.